Random evolution of multiple cracks and associated mechanical behaviors of segmental tunnel linings using a multiscale modeling method

Wang, Fei-Yang; Zhou, Ming-Liang; Zhang, Dong-Ming; Huang, Hong-Wei; Chapman, David

DOI:
10.1016/j.tust.2019.05.008

Document Version
Peer reviewed version

Citation for published version (Harvard):
Wang, F-Y, Zhou, M-L, Zhang, D-M, Huang, H-W & Chapman, D 2019, 'Random evolution of multiple cracks and associated mechanical behaviors of segmental tunnel linings using a multiscale modeling method', *Tunnelling and Underground Space Technology*, vol. 90, pp. 220-230. https://doi.org/10.1016/j.tust.2019.05.008

Random evolution of multiple cracks and associated mechanical behaviors of segmental tunnel lining using a multiscale modeling method

Feiyang Wang[1]，Doctoral student

[1]*Key Laboratory of Geotechnical and Underground Engineering, Department of Geotechnical Engineering, Tongji University, Siping Road 1239 Shanghai, China*

Email: freynwong@163.com

Mingliang Zhou[1]，Doctor

[1]*Key Laboratory of Geotechnical and Underground Engineering, Department of Geotechnical Engineering, Tongji University, Siping Road 1239 Shanghai, China*

Email: zml1608@163.com

Dongming Zhang[1]，Assistant professor

[1]*Key Laboratory of Geotechnical and Underground Engineering, Department of Geotechnical Engineering, Tongji University, Siping Road 1239 Shanghai, China*

Email: 09zhang@tongji.edu.cn

Hongwei Huang[1]，Professor

[1]*Key Laboratory of Geotechnical and Underground Engineering, Department of Geotechnical Engineering, Tongji University, Siping Road 1239 Shanghai, China*

Email: huanghw@tongji.edu.cn

David Chapman[2]，Professor

[2]*Department of Civil Engineering, School of Engineering, University of Birmingham, Birmingham, B15 2TT, UK*

Email: D.N.CHAPMAN@bham.ac.uk

Correspondence should be addressed to Prof. Hongwei Huang; huanghw@tongji.edu.cn

Abstract: Major defects, such as cracks, have significant effects on the mechanical behavior of segmental tunnel linings. However, obvious multiscale phenomena considering the size of cracks and the tunnel structure underestimates its impact on the mechanical behavior of the tunnel lining. Therefore, a novel multiscale modeling method has been proposed in which the potentially damaged and undamaged zones are recognized according to pre-analysis results and then simulated at different scales. In the model, mesoscopic features are considered within potentially damaged zones using a mesostructure cohesive zone method, while the other zones are simulated as a macroscopic homogeneous material. Herein, the mesostructure cohesive zone model has been used to incorporate the mesoscopic components and simulate the random propagation of multiple cracks. This is very useful for characterizing the features of multiple cracks and evaluating the mechanical behavior of segmental tunnel linings. After the multiscale model has been validated using the experimental results, the numerical simulations of the lining segment have been carried out under different loading paths to investigate the evolution characteristics of multiple cracks and their impact on the tunnel lining performance. The study demonstrates that the proposed multiscale model is effective and accurate for modeling the random evolution of multiple cracks and evaluating the load capacity of the segment under different loading paths. The stiffness of the lining was found to be not only dependent on the loading path, but also the features of the crack which in compression dominated segments are dense and narrow and in bending dominated segments are more dispersed and wider. A formula has also been developed to predict crack depth from the observed crack mouth opening displacement. The proposed novel multiscale method is a major step forward in modeling the capacity of cracked concrete tunnel linings.

Keywords: Multiscale modeling method; Multiple cracks; Mesostructure cohesive zone model; Random evolution; Segmental tunnel lining.

1. Introduction

Increasingly serious defects are occurring in tunnels, especially cracks, during the course of their operational lifetimes. Although the mean operational time of the Shanghai metro is less than 10 years, the length of cracks per kilometer reached 4.42m according to statistical data obtained from 365 measurement sections within the Shanghai subway tunnels (Ding, 2016). These data will increase further over time, which may threaten the safety of the segmental tunnel linings. As shown in Fig. 1, there are several main crack

morphologies within the segmental tunnel lining: straight cracks within the standard lining blocks, and diagonal cracks near the springline joints and near the top joint. The integrity and the stiffness of the segmental tunnel lining are reduced by the accumulation of cracks over time.

The studies on cracking of concrete structures incorporate physical tests, theoretical research and numerical simulations. An analytical formula for the short-term crack width and a semi-empirical formula for long-term crack width have been proposed and validated by laboratory experiments (Tan et al., 1995). However, the existing formula for determining crack width is not accurate for segmental tunnel linings (Wang et al., 2011). The numerical research on the effects of crack shape have indicated it is of fundamental importance to consider realistic crack shapes (Branco et al., 2010). The fracture processes of concrete specimens under pure shear and uniaxial tensile stress have been successfully simulated using the discrete element method in which the components of the concrete weren't considered (Iturrioz et al., 2018). Grégoire et al. (2013) carried out three-point bending fracture tests of geometrically similar notched and unnotched specimens. The tests indicated that the load capacity of the concrete beam with an initial fifth-notched is about 40%~50% less than that without a notch. These studies were mainly focused on simple members. However, the mechanical behavior of segmental tunnel linings is different from that of the previous studies as they are a complex compression and bending member, and therefore research is still required for these members.

These defects threaten the structural safety of the segmental tunnel lining, which has prompted an urgent need to study the effect of cracks in segmental tunnel linings. Therefore, the subject of cracking in tunnel linings has become an important topic in recent years. Field testing observations of a shield tunnel in soft clay subjected to unexpected surcharge showed cracks in the crown segment and spalling near the springline segment were found in the inner surface of the segmental tunnel lining (Huang et al., 2017). A geo-mechanical physical model of the tunnel lining under high in-situ stress in the scale 1:50 was built to simulate the constructed tunnel (Lin et al., 2015). In this study, the propagation of cracks and the failure mechanism of the tunnel were better understood from the perspective of the test findings. Lan et al. (2010) investigated cracks in tunnel linings using an elastic-plastic finite element model. The study found that cracks have a significant effect on the deformation and stress distribution within the tunnel lining.

Currently, the research on cracking of tunnel linings mostly uses experiments and monoscale finite element (FE) models. Although experiments can be used to investigate the physical processes involved and FE modeling is able to reveal the regularity of stress and strain at the macroscopic scale, these methods are not good for

problems with multiscale phenomena. The concrete in segmental tunnel linings consists of mortar and aggregate, which exhibits heterogeneous behavior at the mesoscale, especially for cracked concrete. To illustrate the effect of mesoscopic features on the mechanical behavior of concrete, uniaxial tensile tests have been simulated using a homogeneous model and a heterogeneous mesostructure model, respectively. The basic information for these two models including the mesh, the boundary conditions and the fracture parameters were the same. The crack pattern and the stress-strain curves are shown in Fig. 2. There are large differences in the fracture patterns and the stress-strain curves between these two models, as shown in Fig. 2 (a), (b) and (c). The crack in the heterogeneous mesostructure model bypasses the aggregate, which is consistent with what happens in reality. The homogeneous model overestimates the maximum stress by 20% compared to both the model test and the heterogeneous mesostructure model.

The above example indicates that mesoscopic features have a large influence not only on the crack pattern but also on the stress-strain curves, which is consistent with other relevant research (Hansen et al., 1991; Sun and Li, 2016; Yang et al., 2009). Furthermore, the components of the concrete and the cracks are at the millimeter scale. Therefore, it is hypothesized that the cracked segmental tunnel lining in service should be characterized as a multiscale phenomenon in order to capture more accurately its true behavior. In this research, it is worth noting that mesoscale is defined as the scale ranging from nanometer to millimeter, which affects the mechanical behavior of the material. Therefore, to accurately evaluate the performance of segmental tunnel linings, mesoscopic features including crack, aggregate, and mortar should be incorporated into the analysis.

In the field of tunnel engineering, homogeneous models are usually used to obtain structural response for reasons of simplicity and computational efficiency (Katebi et al., 2015). However, this kind of model is not useful when considering the influence of the concrete constituents and random propagation of cracks, which are frequently found in existing segmental tunnel linings. Although, it is inefficient to simulate the mesoscopic features of the entire segmental tunnel lining. Therefore a suitable model is required to take into account both the effect of mesoscopic features, including the components of the concrete and the crack development on the segmental tunnel lining performance, and computational efficiency. In fact, it is not necessary to simulate all the zones with mesoscopic features because most areas of the segmental tunnel lining are undamaged and therefore can be considered as behaving linear elastically. In this case, the influence of microstructures on the behavior of the material can be neglected (Unger and Eckardt, 2011). Therefore, heterogeneous constituents and random propagation of crack only need to be considered in the simulation of damaged or cracked zones, while the

non-damaged zones can be regarded as a homogeneous material for the purposes of computational efficiency.

The objective of this paper is to propose a multiscale modeling method for segmental tunnel linings, which can consider the mesoscopic effects, simulate the random evolution of multiple cracks and evaluate the mechanical behavior of the cracked lining segment. The paper is arranged as follows. In section 2, a multiscale modeling method for segmental tunnel linings is established, and the effectiveness of the model is illustrated by comparing the simulation with the physical model test results. In section 3, the mechanical characteristics of the segmental tunnel lining subjected to ground surface loading are analyzed using a typical ground-structure model. The range of the loading paths for the multiscale model is estimated from this analysis. A multiscale modeling method is then used to study the evolution features of the multiple cracks and the mechanical behavior of the segment under different loading paths. Finally, conclusions are drawn from the results in section 4.

2. Multiscale modeling method for segmental tunnel lining

2.1. Implementation of the multiscale model

A numerical method has been developed to predict crack patterns and load-carrying capacity in which the potential cracks are represented by pre-inserted cohesive interface elements with softening constitutive laws, modeled by a spatially-varying random field (Yang et al., 2009). This method is not capable of considering the physical components of the concrete. The cohesive zone modeling method, which is able to incorporate the physical components of the concrete has been applied into the simulation of uniaxial tests (Wang et al., 2015a; Wang et al., 2015b). However, these studies were mainly focused on a single fracture mode and small scale specimens. However, in practice the fracture mode is usually complex, and the scale of the structure is large. A complete mesostructure FE model inevitably leads to low computational efficiency for large-scale structures. To address these factors, a multiscale method is proposed based on the mesostructure FE method. In this model, the zones where the cracks randomly initiate and propagate are simulated using a mesostructure cohesive zone modeling method. The non-damaged zones are modeled using a homogeneous macroscale method. Details of the multiscale modeling method include the following procedures, and these are shown in Fig. 3.

(1) The potentially damaged zone in which cracks may initiate and propagate is determined by pre-analysis of the whole zone with a macroscale homogeneous model.

(2) The simulation of the potentially damaged zone controlled by mesoscale needs to incorporate mesoscopic features. There are two crucial steps to realize the simulation of the damaged zone. Firstly, the physical components of the concrete are randomly generated in the damaged zone using a bespoke in-house

computer program, where the generated geometric model is meshed with triangular elements. Secondly, cohesive interface elements are inserted into the damaged zone to simulate the initiation and propagation of the cracks.

(3) The fracture properties of the cohesive interface element are first calibrated by uniaxial compression and tension tests, and then the fracture properties are assigned to the cohesive interface elements.

(4) To produce the whole model, the non-damage zone and the damage zone are connected together according to displacement compatibility equations at the interfaces. The model is given boundary conditions and then solved. The process of creating the multiscale model is thus completed.

There are two crucial points in the creation of the multiscale model: determining the location and extent of the damaged zone and the simulation of the random propagation of the cracks. As for the first point, pre-analysis is performed using the homogeneous FE model. In this model, the concrete is assumed to be a trilinearly elastic-plastic material. The potentially damaged zone is distinguished according to the equivalent plastic strain nephogram as elaborated in the next section. Herein, the mesoscale simulation of the potentially damaged zone and the determination of the parameters for these zones are discussed in detail.

2.1.1. Simulation of the damaged zones controlled by mesoscopic features

As mentioned previously, mesoscopic features have a significant effect on the crack patterns and the load-carrying capacity of structural elements and control the mechanical behavior in these zones. After identifying the potentially damaged zone, random initiation and propagation of the cracks in this zone must be simulated. On the other hand, concrete is a multiple media material, consisting of aggregate, mortar and interface transition zones. Therefore, simulating concrete behavior at the mesoscale includes two aspects: the generation of the mesoscopic components and simulation of the cracks.

Based on this starting point, the mesostructure cohesive zone modeling method (MCZM) is utilized to simulate the random propagation of cracks in the potentially damaged zone. The mesoscopic components is primarily generated according to detail information of the aggregate. Aggregate following a Fuller's grading curve is assumed to be elliptical and have a uniform distribution in the potentially damaged zone. This process is completed using an in-house program written in Python, and a geometric model is obtained, as shown in Fig. 4 (a). The geometric model is then meshed by the commercial software ABAQUS. Cohesive interface elements (CIE), which have been employed in the simulation of concrete blocks and beams (Rodrigues et al., 2016; Wang et al., 2015a; Wang et al., 2015b), are inserted into the mesh to simulate the random propagation of cracks. In fact, the propagation of the cracks either propagates inside the mortar or along the interface between the

aggregate and the mortar. Therefore, cohesive interface elements (CIE) are inserted inside the mortar and also between the aggregate and the mortar, as shown in Fig. 4 (b) and (c).

2.1.2. Determination of the parameters for the MCZM

There are several components to be given material parameters, including the mortar, the aggregate, and the CIE inserted inside the mortar and between the aggregate and the mortar. The aggregate and the mortar are assumed to be elastic materials, whose properties are determined according to material tests and are given to the geometric model. The key point is to obtain reasonable material parameters for the CIE. To be conveniently and efficiently, a bilinear traction-separation criterion is adopted for the CIE to simulate the crack propagation in the concrete, as shown in Fig. 5.

The damage evolution for the bilinear traction-separation criterion is described by a damage variable D (Camanho and Davila, 2002). D is calculated using Eq. (1).

$$D = \frac{\delta(\delta_f - \delta_0)}{\delta_f(\delta - \delta_0)} \tag{1}$$

where δ_0 and δ_f are the effective damage initiation displacement and the failure displacement, respectively. The displacement δ is determined during analysis using the BK fracture criterion (Benzeggagh and Kenane, 1996) described in Eq. (2). This fracture criterion is suitable for the same critical fracture energies in the first and the second shear directions.

$$G_{TC} = G_n^C + (G_s^C - G_n^C)\left\{\frac{G_s}{G_s + G_n}\right\}^{\eta} \tag{2}$$

where G_S , G_n are energy release rates in the shear direction and normal direction respectively. G_s^C and G_n^C refer to the corresponding fracture toughness of the shear fracture and tension fracture. According to the BK criterion, Eq. (2) is converted into Eq. (3) to estimate δ.

$$\delta = \frac{2}{K_0\delta_0}\{G_n^C + (G_s^C - G_n^C)\left\{\frac{\delta_s^{\,2}}{\delta_s^{\,2} + \delta_n^{\,2}}\right\}^{\eta}\} \tag{3}$$

where δ_s and δ_n are displacements in the shear direction and normal direction, and η is a material parameter.

To determine the above-mentioned parameters, uniaxial tension and compression tests are performed with MCZM being used to inverse the material properties (Unger and Eckardt, 2011; Akita et al., 2003). It is worth

noting that the material properties of the CIE between the aggregate and the mortar are different from those of the CIE inside the mortar, to allow for the weaker interface between the aggregate and the mortar. The difference between these two CIEs are described in research conducted by Rodrigues et al. (2016). Based on this approach, the material parameters can be successfully estimated and have been shown to be consistent with test results (Fig. 6). The final parameters are listed in the Table 1. The results shown in Fig. 6 also reveal that the MCZM is accurate and useful for simulating the random propagation of tensile and compressive cracks.

2.2. Validation of multiscale model by segmental loading test

In order to validate the proposed model, the results of the model are compared with those obtained from a segment loading test. A schematic of the segmental loading test is shown in Fig. 7. The equipment shown in Fig. 7 is the segment loading system TJGPJ-2000 (Sun, 2018). The segment is hinged at the ends and loaded by vertical and horizontal jacks. The loading path is controlled by setting the ratio of the vertical load to the horizontal load.

Before establishing the multiscale model, a pre-analysis is conducted by using a homogeneous model to identify the potentially damaged zone of the multiscale model. The same loading path as the test is applied to the model. The segment in the homogeneous model is regarded as a tri-linearly elastic-plastic material. After conducting the homogeneous model analysis, the equivalent plastic strain nephogram under the limit state is produced, as illustrated in Fig. 8 (a). It is highly likely that the zone showing plastic strains is damaged, and therefore this zone is simulated with the MCZM and the other zones are still assumed to be homogeneous. Finally, the multiscale model of segment shown in Fig. 8 (b) is formulated according to the implementation process previously described. The parameters in the mesoscale and macroscale are presented in Table 1.

2.2.1. Random propagation of the multiple cracks

The multiscale model with the same loading path as the experiment is then analyzed. The final cracked states in the experiment and in the simulation are shown in Fig. 9 (a) and (b). During the numerical simulation, it was found that the crack path was different for different segments analyzed. This phenomenon often occurs in physical experiments, but it is interesting to note this also occurs in the multiscale simulations. This shows that the mesostructure of the segment, such as the distribution of the aggregates, directly influences the crack path.

According to the results of the test and the simulation, multiple cracks initiate vertically and then propagate in the area between the loading beams. Several cracks propagate once the first crack has been initiated. The propagation process of the cracks in the simulation is in good agreement with that in the test. According to the

simulation and the test, there are several distinct features in the propagation process of the cracks. At the initial fracture stage, the cracks expand vertically upwards, appearing as I-type cracks. The cracks at this stage are mainly located in the tensile zone of the segment, resulting from the tensile stress. Towards the final stages of the loading, Y-type cracks emerge. The reason for the Y-type cracks is that the cracks move up to the compression zone and the concrete is subjected to both tension and compression stresses and hence they are mixed mode cracks. In general, the multiscale model proposed in this paper is able to simulate random propagation of multiple cracks.

2.2.2. Mechanical behavior of the cracked segment

The crack growth laws of the loading test are basically consistent with those obtained by the multiscale model. To describe the mechanical behavior of the segment, graphs of the internal forces and deformations from the test and the simulation are plotted in Fig. 10. The bending moment-deflection curves of two mid-span monitoring points during the test and one point in the multiscale model at the mid-span are shown in Fig. 10 (a). In addition, the crack with the maximum opening has been selected as an analysis object. The bending moment–crack mouth opening displacement (CMOD) curves for this crack are plotted in Fig. 10 (b). The stars in the figure indicate the occurrence of the I-type cracks and Y-type cracks. The curves reveal that the bending moment increases nonlinearly with the growth of the cracks. When the bending moment reaches 70kN·m and 145kN·m, I-type cracks and Y-type cracks occur, respectively. The bending moment increases slightly with the expansion of the crack because the cracked concrete has failed. In general, the curves obtained from the simulation are essentially in line with those obtained from the experiment. The curves also indicate that the relationship between the internal forces and the deformation is complicated.

Based on the evolution laws of the cracks and the curves shown in Fig. 10, the mechanical behavior of the segment can be described in three stages: non-cracked (linear state), I-type cracks develop (non-linear stage) and Y-type cracks develop (failure stage). In the first loading stage, there are no cracks and the deflection of the segment increases linearly with the bending moment. In the second loading stage, multiple cracks initiate and propagate, which results in the deflection or CMOD increasing nonlinearly with the bending moment. The slope of the bending moment–deflection or –CMOD curves decreases slightly with loading during this stage. The Y-type cracks start propagating when the segment enters the third loading stage. Simultaneously, the gradient of the bending moment–deflection or –CMOD curves decreases sharply with loading. Furthermore, the bending moment–deflection curves illustrate that the stiffness only decreases slightly with loading during the first two

stages, while the stiffness decreases rapidly after the emergence of the Y-type cracks.

Before the emergence of the Y-type cracks, the stiffness of the segment decreases nonlinearly with loading and the damaged stiffness is less than half of the initial stiffness. It is therefore important to consider the influence of multiple cracks on the stiffness. According to the above analysis, the bending moment can be used as a surrogate for the load capacity when the Y-type crack emerges. Therefore, the bending moment at the first sign of the Y-type crack can be regarded as the ultimate load capacity.

3. Multiscale analysis of the segmental tunnel lining

3.1. Determining the load path

3.1.1. Typical ground-structure model

In this section, the proposed multiscale model has been used to analyze the mechanical behavior of the complete segmental tunnel lining under surface loading. To achieve this, the loading path experienced by the segmental tunnel lining under surface loading is estimated using a typical ground-structure model. The proposed multiscale modeling method is then conducted to evaluate the performance of the segmental tunnel lining based on the estimated loading path.

Ground-structure models have been extensively used in the past, for example Katebi et al. (2015), Lambrughi et al. (2012) and Mollon et al. (2012). Herein, the model has been used to estimate the load path experienced by the segmental tunnel lining under surface loading. The ground-structure model is presented in Fig. 11, in which the overburden of the tunnel is three times the tunnel diameter (D). The dimensions of the model have been chosen to minimize the boundary effects and improve the computational efficiency (Lambrughi et al. 2012). The model extends to a depth of three times the tunnel diameter (D) below the tunnel invert and laterally to a distance of 5.5D from the tunnel centerline. There are four steps in the analysis: initiation of the geostatic stress, excavation of the tunnel, installation of the segmental tunnel lining and application of the surface loading.

The soil was simulated with 4-node first order reduced integration elements (CPE4R), and the soil behavior was assumed to be governed by an elastic perfectly-plastic constitutive relationship based on the Mohr-Coulomb criterion with a non-associative flow rule. To simplify the analysis, only one soil layer was taken into account in the model, and the parameters are listed in Table 2. The segmental tunnel lining is consisted of six segments, as shown in Fig. 11 (b). The segmental tunnel lining was modeled using an elastic-plastic material. Relative motion was allowed between adjacent tunnel segments and between the segments and the soil. Therefore, contact

288 friction was adopted for this behavior. The node-surface contact was set up between the segments and
289 surrounding soil, and between adjacent segments. The normal and tangential behaviors of the contact are
290 governed by an isotropic Coulomb friction model and a hard contact model, respectively.

291 **3.1.2. Internal forces in the segmental tunnel lining under surface loading**

292 The segmental tunnel lining under surface loading was analyzed with the typical ground-structure model.
293 The curves of internal force to surface load at the 0°, 30°, 90°, 8° joint, 73° joint and 138° joint were obtained
294 and have been plotted in Fig. 12. The positive bending moment denotes that the inside surface of the segmental
295 tunnel lining is subject to tension. The axial force has been taken as positive when the cross section of the lining
296 was subject to compression. As expected, the axial forces and the bending moments increase at different
297 gradients for different locations as the surface loading increases. The maximum axial force and the maximum
298 bending moment occur at the 73° joint. As shown in Fig. 12 (b), the inner surface at the 73° joint and at 90° is
299 subject to compression, and the inner surface of the other sections is subject to tension. Meanwhile, the bending
300 moment at the 138° joint is very small, which means the lining near to the 138° joint is mainly in compression.

301 The axial force, the bending moment and the ratio of bending moment to axial force under a surface load of
302 500kPa around the circumferential section of the segmental tunnel lining are shown in Fig. 13. The profile of the
303 segmental tunnel lining is plotted to show the magnitude of the values. A positive axial force denotes the lining is
304 subject to compression, and a positive bending moment is drawn in the tension side of the segmental tunnel
305 lining. Fig. 13 (a) indicates that the whole lining is subject to compression. The axial force in the standard blocks
306 is larger than for the other blocks, and the lowest axial force is in the bottom block. The bending moment in the
307 bottom block, the top block and part of contiguous blocks causes tension on the inside surface, as shown in Fig.
308 13 (b). The bending moment is negative in the lining near the springline joint, including within the contiguous
309 blocks and standard blocks. The ratio of the bending moment to axial force is presented in Fig. 13 (c) and ranges
310 from 0 to 0.3. The figure shows there are relatively large ratios of the segmental tunnel lining located at the top
311 and the bottom parts of the segmental tunnel lining. That is to say, the sections at the top and the bottom part of
312 the segmental tunnel lining are subject to both compression and bending, while other sections of the lining are
313 mainly in compression.

314 From the above analysis, the internal force in the segmental tunnel lining varies differently for different
315 sections. The ratio of bending moment to axial force at the top and the bottom part of the segmental tunnel lining
316 is relative large, and these members are regarded as compression-bending members. As we know, the bending

capacity of concrete members is much less than the compressive capacity and hence these sections with large ratios are vulnerable. From another perspective, the segmental tunnel lining is classed as damaged, e.g. spalling and cracks, in practical engineering under extreme surface load (Huang et al., 2017). Cracks are often found in the top part of the segmental tunnel lining in service as confirmed on site by images captured by tunnel inspection equipment (Huang et al., 2018). However, there is no decrease in the load capacity from the results obtained from the ground-structure model. The reason for the results is that the segmental tunnel lining is assumed to be an elastic-plastic material, which is not capable of reflecting an accurate mechanical response for the segmental tunnel lining under the extreme surcharge. Therefore, as it is demonstrated that the sections at the top part of the segmental tunnel lining are vulnerable and these must be investigated with the proposed multiscale modeling method.

3.1.3. Loading path

According to the calculation results, the loading path for the multiscale model has been estimated using the following process. The ratio of the bending moment to the surface load and the ratio of the axial force to the surface load are denoted by $k_M=M/P_{load}$ and $k_N=N/P_{load}$, respectively, where P_{load} is the surface load and M and N are the bending moment and axial force determined from the ground-structure model. After a series transformation, Eq. (4) is obtained to determine the loading path for the multiscale model with respect to the corresponding ground-structure model:

$$P / N = (k_M / k_N + h) / l = (e + h) / l \tag{4}$$

where P, N, h and l are the physical parameters of the multiscale model shown in Fig. 8, and $e=M/N$ is eccentricity distance.

According to the results from the ground-structure model and Eq. (1), P/N of the vulnerable section is equal to 0.65. In order to investigate the effects on the performance of the segmental tunnel lining, values of P/N of 0.55, 0.60, 0.65, 0.70 and 0.75 are used with the multiscale model.

3.2. Results analysis

To characterize the random propagation of the multiple cracks and the mechanical behavior, the segment under different loading paths has been analyzed using the multiscale model. The cracking and the loading path are significant factors affecting the performance of the segmental tunnel lining in service. Therefore, the crack pattern and the effect of the multiple cracks on the performance of the segmental tunnel lining under the

346 specified loading paths have been investigated.

347 **3.2.1. Evolution features of multiple cracks**

348 Fig. 14 shows the cracking states under different loading conditions with values of *P/N* equal to 0.55, 0.60,
349 0.65, 0.70 and 0.75, respectively. The actual value of *P/N* indicates the eccentricity distance for the segment
350 section. As *P/N* increases, the segment gradually transits from being compression dominated to bending
351 dominated. The cracks are mainly distributed between the loading beams under the different loading paths. More
352 cracks develop when the eccentricity distance is larger. However, the crack mouth opening displacement
353 (CMOD) of the segment with the larger eccentricity is greater for a given bending moment. The simulation
354 results at failure showed that the cracks in the compression dominated segment are dense and narrow, while
355 those of the bending dominated segment are more dispersed and wider.

356 Dissipation energy due to damage is useful to quantitatively describe the characteristics of multiple cracks.
357 This quantity has been used to interpret the cracking behavior of industrial ceramics, which is a quasi-brittle
358 material (Leplay et al., 2011). Therefore, to further understand the crack evolution, it is proposed to quantify the
359 damage dissipation energy (DDE) of the segment under different loading paths. Herein, the DDE obtained from
360 the multiscale model is the release energy of the whole model due to damage. The curves of DDE versus the
361 vertical load on the segment under different loading conditions are plotted in Fig. 15. The star marks in Fig. 15
362 denote the first appearance of the Y-type cracks. For all the loading paths, the DDE increases nonlinearly with
363 loading after damage. The release of DDE goes up with an increase in *P/N*. During the initial loading stage, the
364 DDE is zero, which indicates that there is no damage in the segment. After this, the DDE release accelerates with
365 the loading. As the Y-type cracks occur, the DDE increases sharply, which indicates failure of the segment.

366 The energy dissipated by damage is a useful tool to describe the failure process of the segment and
367 quantitatively characterize the failure differences of a segment under different loading paths. The above analysis
368 shows that the DDE becomes larger at the same load level as an axial compression dominated member gradually
369 changes into a bending dominated member. An abrupt increase in the DDE with loading is an obvious sign to
370 predict the failure of the segment.

371 **3.2.2. Mechanical behavior of the segment with crack evolution**

372 The curves of the bending moment versus deflection in the mid-span section are plotted in Fig. 16. For
373 different loading paths, the bending moment increases with deflection at different gradients. The gradient of the
374 bending moment–deflection curve is large for small eccentricities, which is beneficial for improving the bending

stiffness of the section. The curves can be divided into three stages according to the discussion in the previous section. During the first stage, the loading path makes little influence to the moment–deflection curves. During the last two stages, the effect of the magnitude of the eccentricity becomes gradually more significant with loading. It is easy to show that the maximum bending moment increases with a reduction in the eccentricity from the curves. The curves also indicate that the stiffness of the segment gradually degrades after cracking. This situation is obvious for large eccentricities.

The moment–deflection curves show that the stiffness of the segment is not only dependent on the loading path, but also on the development of the cracks. Before the presence of the cracks, the stiffness of the segment has a minimal relationship to the loading path. During the cracking stage, however, the stiffness declines with increasing eccentricity. When the Y-type cracks appear, the stiffness of the segment decreases sharply. Herein, the authors suggest that the bending moment at the presence of a Y-type crack can be regarded as the ultimate load capacity, which is also illustrated by the DDE–load curves. As mentioned previously, the stiffness of the segment depends on the crack evolution and the loading path. If a homogeneous monoscale model is used to simulate the cracked segmental tunnel lining, the stiffness of the segment should be reduced according to both the crack state and the loading path.

To reveal the evolution law of the cracks under different loading conditions, the curves of the bending moment in the mid-span section to the CMOD and to the length of the crack are shown in Fig. 17. As shown in Fig. 17 (a), the relationship between the CMOD and the bending moment is nonlinear. There is a minimal difference in the cracking moment for the different loading paths. At the initial cracking stage, the CMOD increases slightly with the increase in bending moment and then increases sharply after the CMOD reaches 0.35mm. After the presence of the Y-type cracks, the bending moment of the segment remains almost constant with loading and the CMOD of the crack develops rapidly. The crack depth increases with an increase in bending moment of the segment as shown in Fig. 17 (b). Moreover, the required bending moment is improved as P/N increases for the same value of crack depth. In general, the crack evolution, including CMOD and crack depth, is difficult for the small eccentricities for which the required bending moment is large.

Although there are large differences in the bending moment–CMOD or –crack depth curves, the relationship between the crack depth and the CMOD shows minimal change for different loading paths. The curves of crack depth to CMOD under different loading paths are shown in Fig. 18. The crack depth initially grows quickly with an increase in CMOD. After the CMOD goes beyond 0.3mm, but remains less than 1.0mm, the crack depth

slows down as the CMOD increases. The crack depth then increases very slowly with an increase in crack opening. It is hard to detect the crack depth for an underground structure, especially in segmental tunnel linings. Therefore, a logarithmic form of the prediction formula for the crack depth shown in Eq. (5) is proposed according to the characteristics of the crack evolution.

$$L_{cd} = 6.55\ln(46L_{cm} + 0.98) \quad (R^2=0.98) \tag{5}$$

where L_{cd} and L_{cm} are the crack depth and the crack mouth opening displacement, respectively. R^2 is the correlation coefficient of the predicted results and the simulation results.

The curve of the prediction formula shown in Fig. 18 is close to the simulation results with a correlation coefficient of 0.98. The formula is very helpful for predicting the crack depth from the measured CMOD value.

4. Conclusions

The novel multiscale modeling method proposed in this research has revealed the random evolution of multiple cracks and investigated the mechanical behavior of the segment under different loading paths. It has been shown that the proposed model is effective and accurate at describing the evolution characteristics of multiple cracks, and offers a major step forward in modeling the capacity of cracked concrete segmental tunnel linings. Meanwhile the relationship between the bending moment and crack features obtained by the proposed model has been analyzed in this study. A new prediction formula for the crack depth has been proposed relating crack depth to the crack mouth opening displacement. According to the multiscale simulation of the segment under different loading conditions, the evolution characteristics of multiple cracks and the mechanical behavior of the segment can be concluded as follows:

(1) There are three stages for the cracking under the surface loading condition: non-crack (linear state), I-type crack (non-linear stage) and Y-type crack (failure stage). Cracks in bending dominated segments with small eccentricities are dense and narrow, while those in bending dominated segments with large eccentricities are more dispersed and wider.

(2) The load capacity of the segment increases with a reduction in the eccentricity. The energy dissipated by damage is an available and quantitative index to predict the failure of segments with different eccentricities.

(3) The stiffness of the segment is not only dependent on the loading path, but also on the crack features. The influence of the loading path and the crack features on the stiffness of the segment gradually increases with loading.

(4) The loading path has minimal effect on the relationship between the crack mouth opening displacement

and the crack depth. The proposed formula is effective and accurate at predicting the crack depth from the crack mouth opening displacement.

The random evolution characteristics of multiple cracks and the mechanical behavior of segment have been investigated successfully using the proposed multiscale modeling method presented in this paper. However, the joints of the segmental tunnel lining have not been involved in the multiscale modeling. Therefore, the authors intend to use the proposed method to investigate the effects of the joints on the segmental tunnel lining in future work.

Acknowledgments

The study has been supported by the Natural Science Foundation Committee Program of China (No. 51538009 & No. 5153000295). This financial support is gratefully acknowledged.

References

Akita, H., Koide, H., Tomon, M., Sohn, D., 2003. A practical method for uniaxial tension test of concrete. Materials & Structures 36, 365-371.

Benzeggagh, M.L., Kenane, M., 1996. Measurement of mixed-mode delamination fracture toughness of unidirectional glass/epoxy composites with mixed-mode bending apparatus. Composites Science & Technology 56, 439-449.

Branco, R., Rodrigues, D.M., Antunes, F.V., 2010. Influence of through‐thickness crack shape on plasticity induced crack closure. Fatigue & Fracture of Engineering Materials & Structures 31, 209-220.

Camanho, P.P., Davila, C.G., 2002. Mixed-Mode Decohesion Finite Elements for the Simulation of Delamination in Composite Materials.

Ding, W., 2016. Safety assessment method of shield tunnel structures in soft soil. Tongji university. (in chinese)

Grégoire, D., Rojas-Solano, L.B., Pijaudier-Cabot, G., 2013. Failure and size effect for notched and unnotched concrete beams. International Journal for Numerical & Analytical Methods in Geomechanics 37, 1434–1452.

Hansen, A., Hinrichsen, E.L., Roux, S., 1991. Scale-invariant disorder in fracture and related breakdown phenomena. Physical Review B Condensed Matter 43, 665-678.

Huang, H., Shao, H., Zhang, D., Wang, F., 2017. Deformational responses of operated shield tunnel to extreme surcharge: a case study. Structure & Infrastructure Engineering 13, 345-360.

Huang, H.W., Li, Q.T., Zhang, D.M., 2018. Deep learning based image recognition for crack and leakage defects of metro shield tunnel. Tunnelling & Underground Space Technology 77, 166-176.

Iturrioz, I., Birck, G., Riera, J.D., 2018. Numerical DEM simulation of the evolution of damage and AE preceding failure of structural components. Engineering Fracture Mechanics.

Katebi, H., Rezaei, A.H., Hajialilue-Bonab, M., Tarifard, A., 2015. Assessment the influence of ground stratification, tunnel and surface buildings specifications on shield tunnel lining loads (by FEM). Tunnelling and Underground Space Technology incorporating Trenchless Technology Research 49, 67-78.

Lambrughi, A., Rodríguez, L.M., Castellanza, R., 2012. Development and validation of a 3D numerical model for TBM–EPB mechanised excavations. Computers & Geotechnics 40, 97-113.

Lan, W., Deng, X., Sutton, M.A., 2010. Investigation of crack tunneling in ductile materials. Engineering Fracture Mechanics 77, 2800-2812.

Leplay, P., Réthoré, J., Meille, S., Baietto, M.C., 2011. Identification of damage and cracking behaviours based on energy dissipation mode analysis in a quasi-brittle material using digital image correlation. International Journal of Fracture 171, 35-50.

Lin, P., Liu, H., Zhou, W., 2015. Experimental study on failure behaviour of deep tunnels under high in-situ stresses. Tunnelling & Underground Space Technology Incorporating Trenchless Technology Research 46, 28-45.

Mollon, G., Dias, D., Soubra, A.H., 2012. Probabilistic analyses of tunneling-induced ground movements. Acta Geotechnica 8, 181-199.

Rodrigues, E.A., Manzoli, O.L., Jr, L.A.G.B., Bittencourt, T.N., 2016. 2D mesoscale model for concrete based on the use of interface element with a high aspect ratio. International Journal of Solids & Structures 94–95, 112-124.

Sun, B., Li, Z., 2016. Multi-scale modeling and trans-level simulation from material meso-damage to structural failure of reinforced concrete frame structures under seismic loading. Journal of Computational Science 12, 38-50.

Sun, Y., 2018. Study on subway tunnel lining defects inspection system and cracked tunnel structural safety assessment. Tongji university. (in chinese)

Tan, K.H., Paramasivam, P., Tan, K.C., 1995. Cracking characteristics of reinforced steel fiber concrete beams under short- and long-term loadings. Advanced Cement Based Materials 2, 127-137.

Unger, J.F., Eckardt, S., 2011. Multiscale modeling of concrete. From mesoscale to macroscale. Archives of Computational Methods in Engineering 18.

Wang, J., Leng, F., Jiang, Y., 2011. Study on Behavior and RCFEM Designing of Restricting Crack Width of Circular Pressure Tunnel Lining, Geohunan International Conference, pp. 162-169.

Wang, X., Yang, Z., Jivkov, A.P., 2015a. Monte Carlo simulations of mesoscale fracture of concrete with random aggregates and pores: a size effect study. Construction & Building Materials 80, 262-272.

Wang, X.F., Yang, Z.J., Yates, J.R., Jivkov, A.P., Zhang, C., 2015b. Monte Carlo simulations of mesoscale fracture modelling of concrete with random aggregates and pores. Construction & Building Materials 75, 35-45.

Yang, Z.J., Su, X.T., Chen, J.F., Liu, G.H., 2009. Monte Carlo simulation of complex cohesive fracture in random heterogeneous quasi-brittle materials. International Journal of Solids & Structures 46, 3222-3234.

Table and figure lists

535 Table 1. Material properties for the multiscale model.

Materials	Elastic modulus /GPa	Tensile strength /MPa	Shear strength /MPa	Poisson's ratio	Fracture energy (I) kN/m	Fracture energy (II) kN/m
Aggregate	70	-	-	0.16	-	-
Mortar	25	-	-	0.22	-	-
Mortar-mortar interface	100000	4	25	-	0.18	8.00
Mortar-aggregate interface	100000	3	15	-	0.12	5.00
Concrete	32			0.18		

536
537
538 Table 2. Geotechnical properties for the soil layer in the model.

Soil type	Depth /m	Density γ (kN/m^3)	Elastic modulus E (kPa)	Cohesion c (kPa)	Friction angle φ (°)	Dilation angle (°)
Clay ⑤-1	42.0	18.3	20000	21.0	12.5	0

539 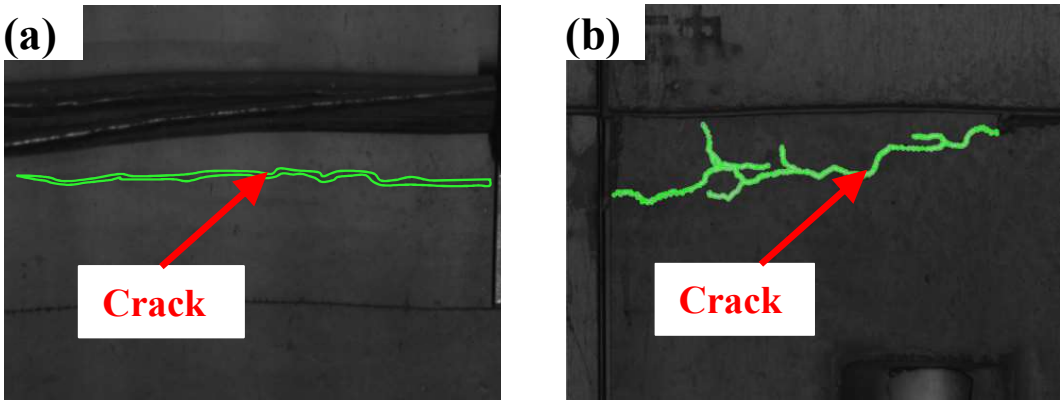

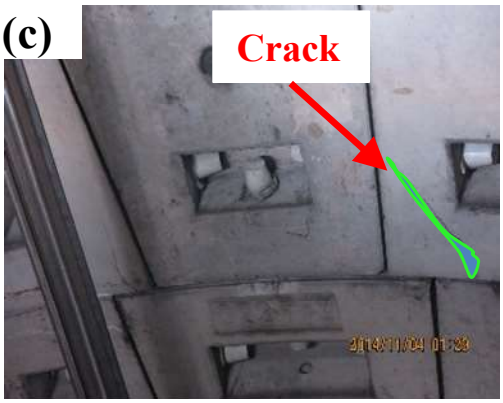

540

541 Fig. 1. Crack morphology of segmental tunnel linings in service. (a) Crack in standard lining segment; (b)
542 Springline crack; (c) Crown crack.

543

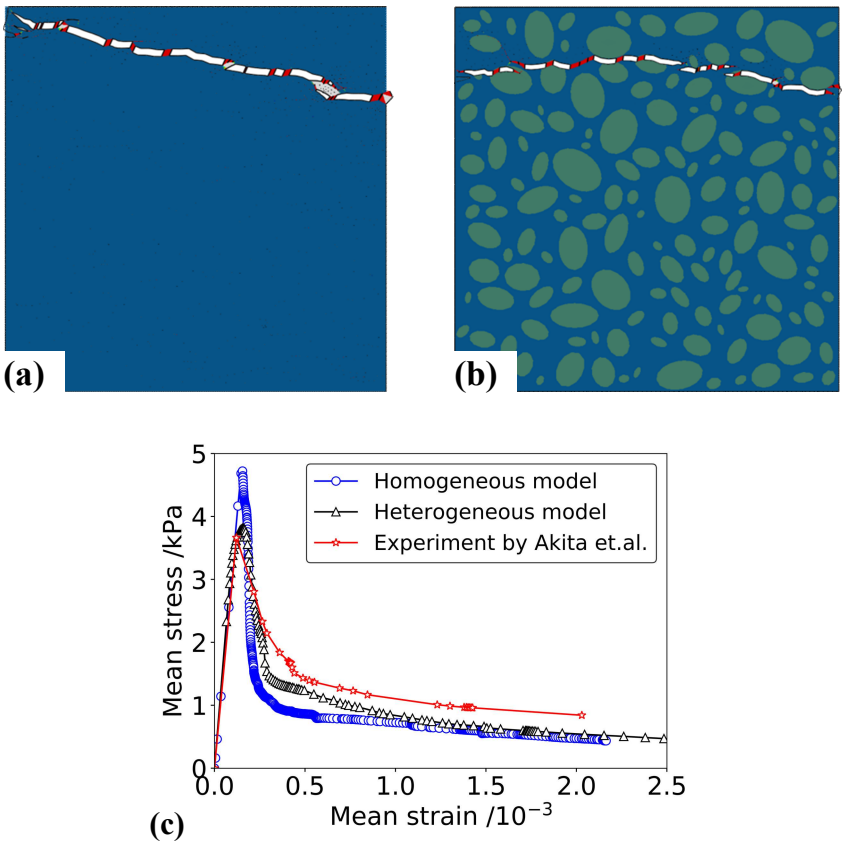

Fig. 2. Uniaxial tensile failure of a concrete specimen. (a) Crack formed in the homogeneous model; (b) Crack formed in the heterogeneous model; (c) Curves of stress-strain for both models compared to experimental data.

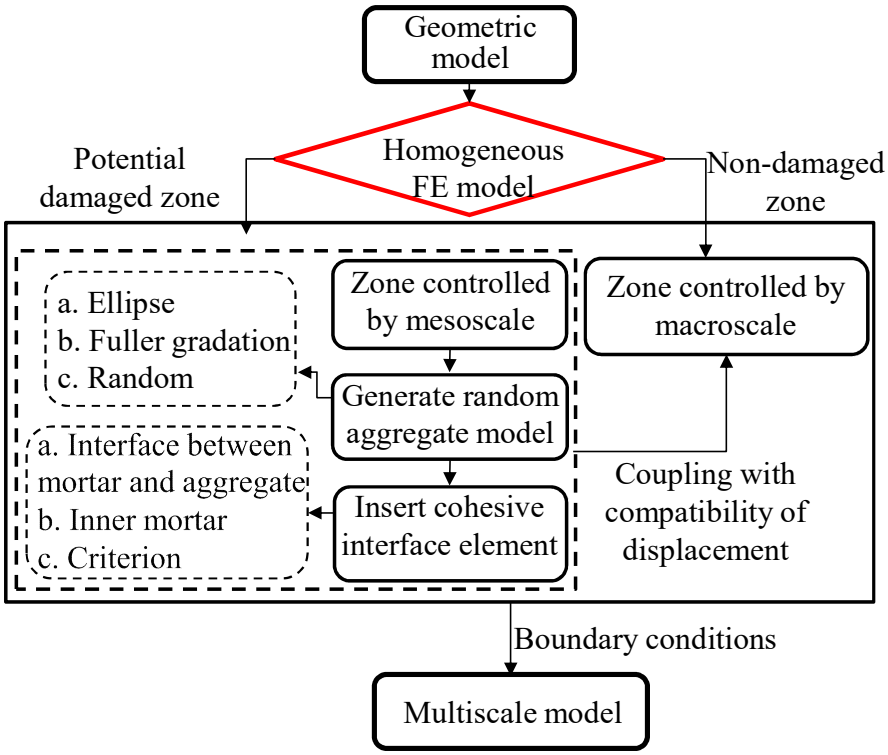

550

551 Fig. 3. Flow chart for the multiscale modeling method.

552

553

554

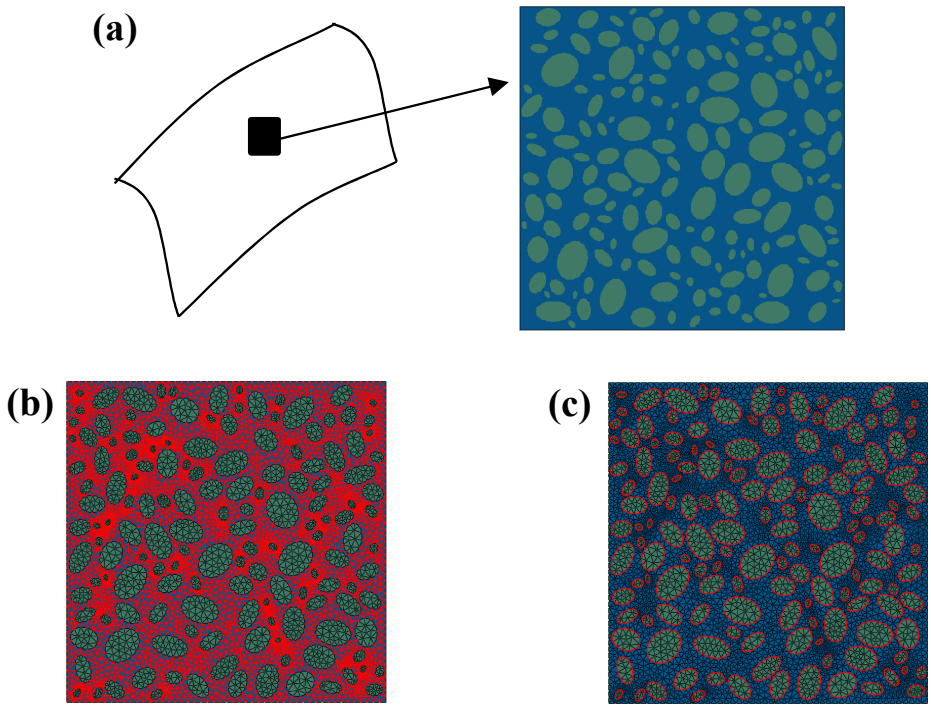

555

556 Fig. 4. Mesostructure cohesive zone model. (a) Geometric model; (b) CIE between the mortar and the aggregate;

557 (c) CIE inside the mortar. (The mesh marked in red is CIE.)

558

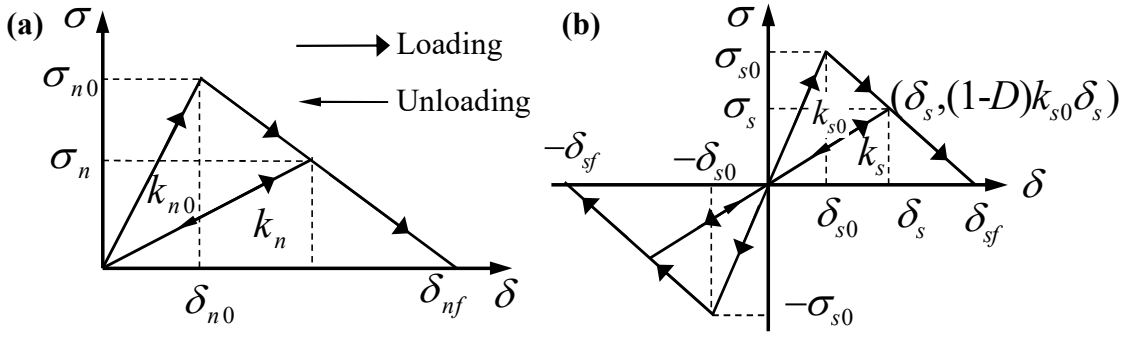

559

560 Fig. 5. Traction-separation criterion for a cohesive interface element. (a) Tension; (b) Shear.

561

562

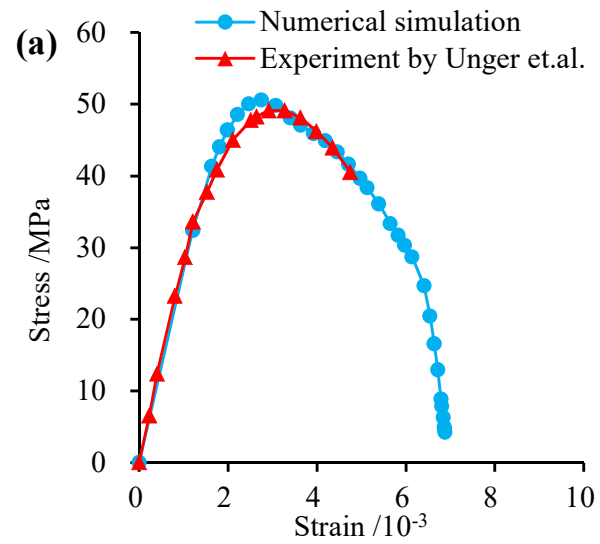

563

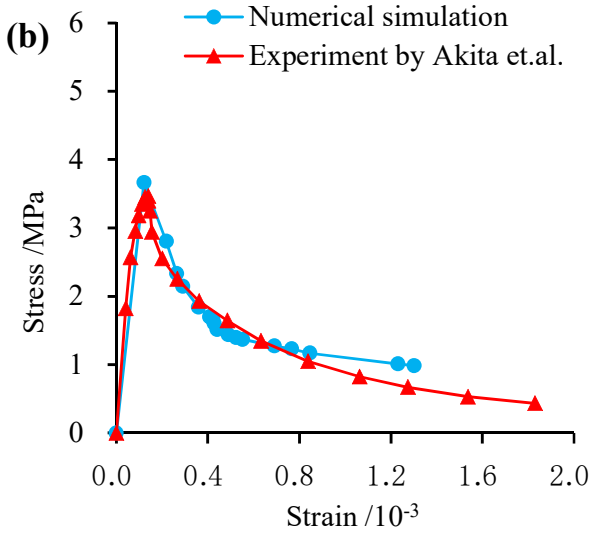

564

565 Fig. 6. Uniaxial test to determine the parameters for the CIE. (a) Uniaxial compressive test; (b) Uniaxial tensile

566 test.

567

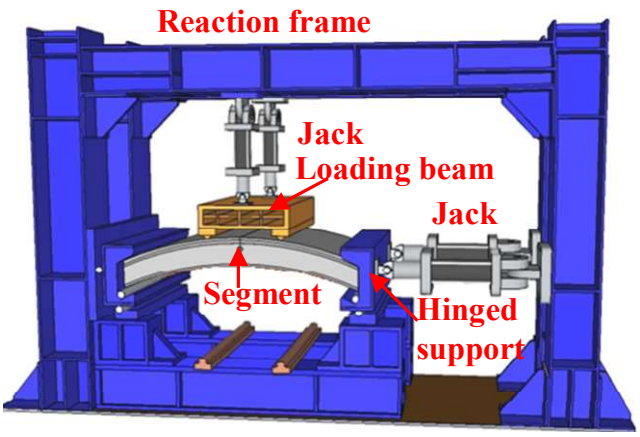

568
569
570 Fig. 7. Schematic of the segmental loading test.
571

572

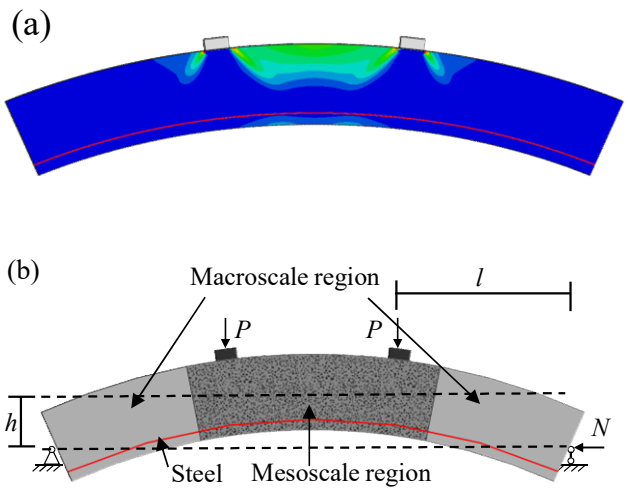

573

574 Fig. 8. Realization of the multiscale model. (a) Equivalent plastic strains; (b) Multiscale model.

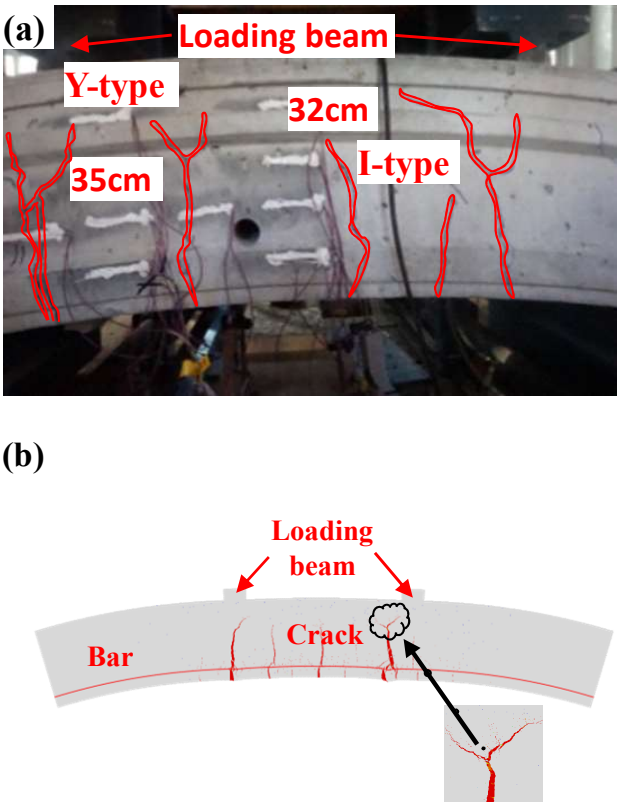

Fig. 9. Cracks at failure in the concrete segment. (a) Loading test; (b) Numerical simulation (scaling factor of 20).

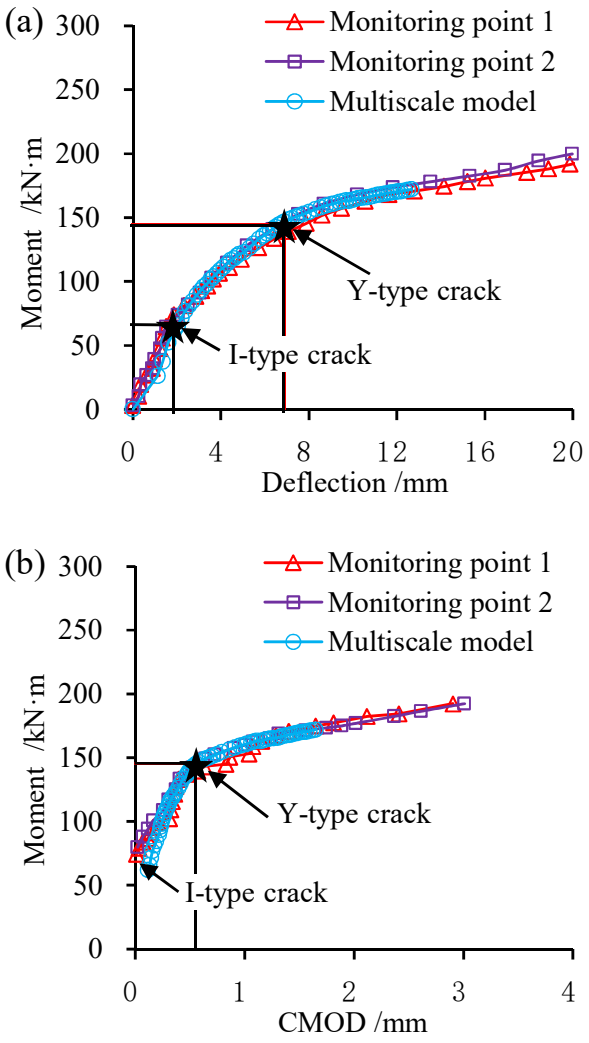

Fig. 10. Comparison between the numerical and experimental results. (a) Moment-deflection curves; (b) Moment-CMOD curves.

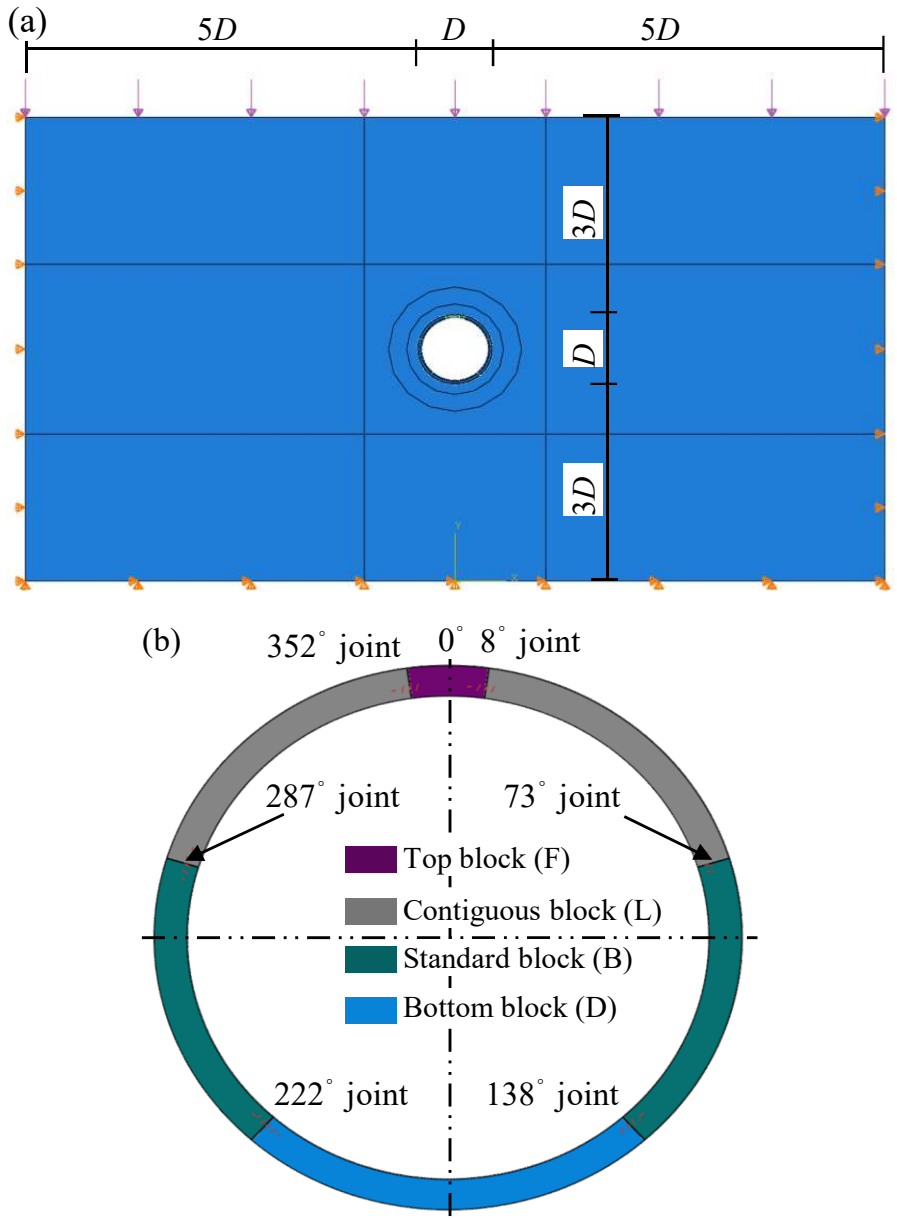

588

589

590 Fig. 11. Schematic diagram of the ground-structure model. (a) Ground-structure model; (b) Segmental lining.

591

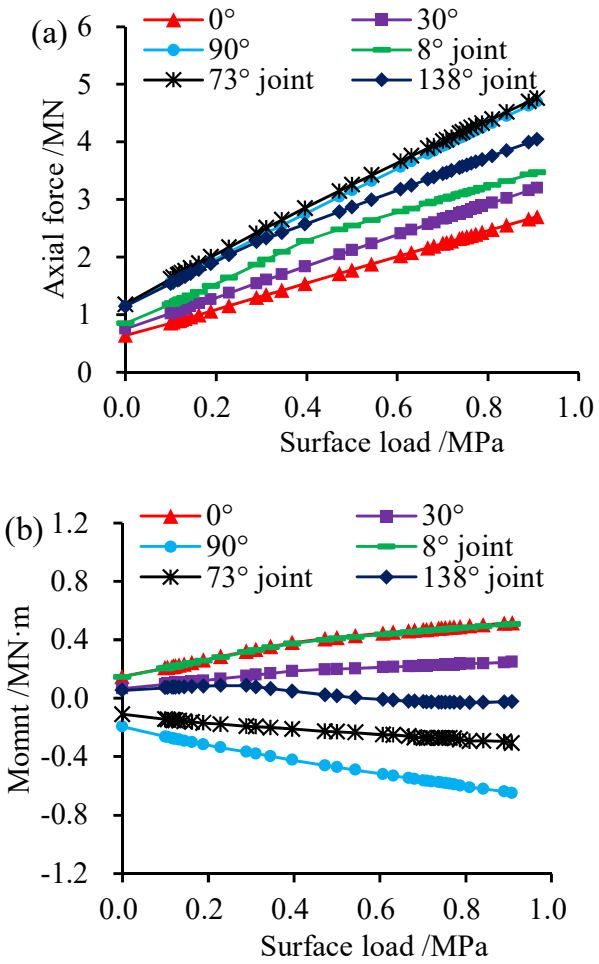

Fig. 12. Curves of internal force with surface load. (a) Axial force; (b) Bending moment.

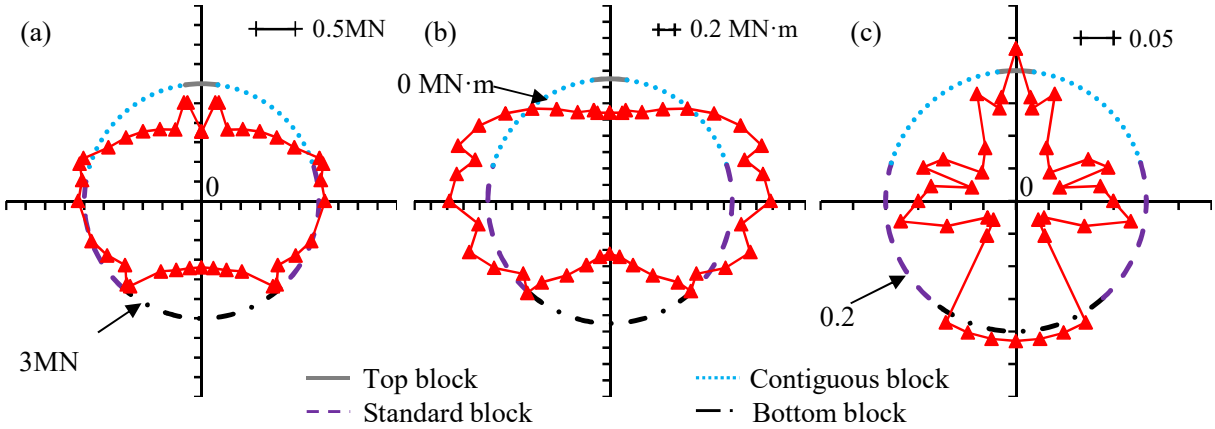

596

597 Fig. 13. Internal forces in the tunnel lining. (a) Axial force; (b) Bending moment; (c) Ratio of the bending moment
598 to the axial force.

599

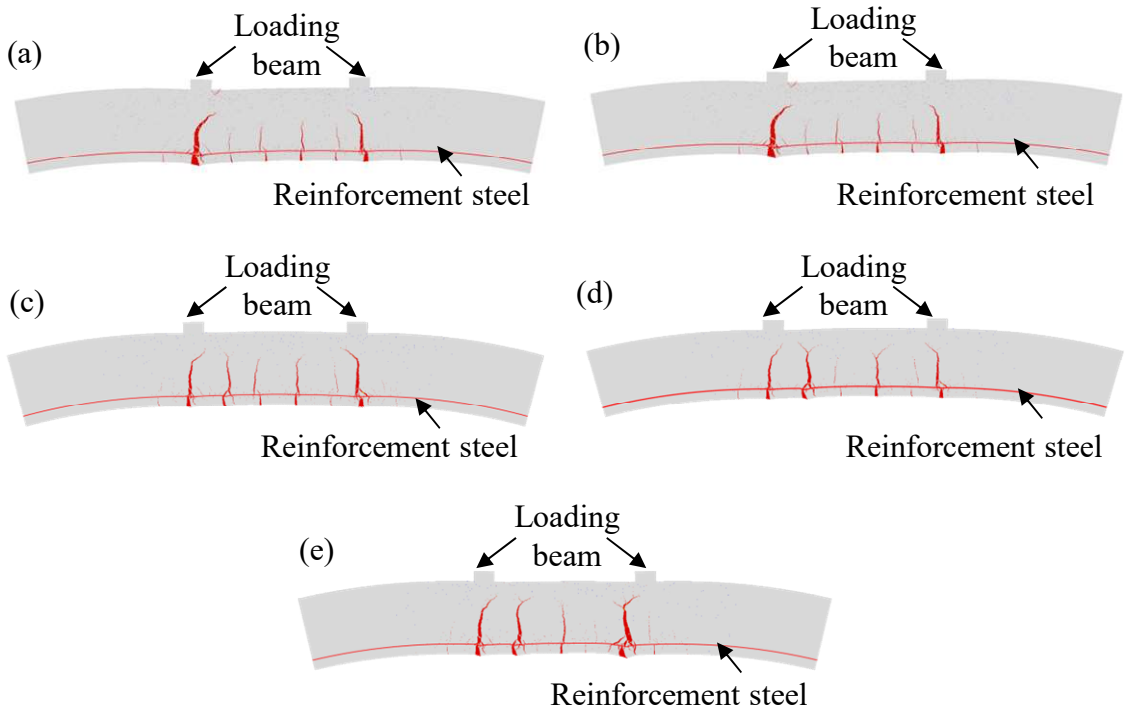

Fig. 14. Cracking states under different loading conditions (scaling factor of 10). (a) P/N=0.55; (b) P/N=0.60; (c) P/N=0.65; (d) P/N=0.70; (e) P/N=0.75.

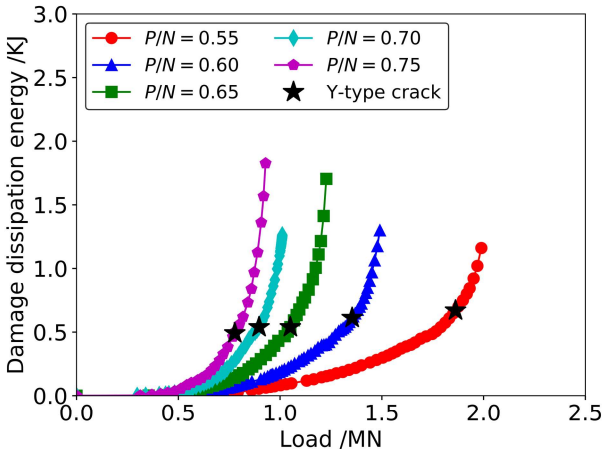

607

608 Fig. 15. Energy dissipated by damage under different loading paths.

609

610

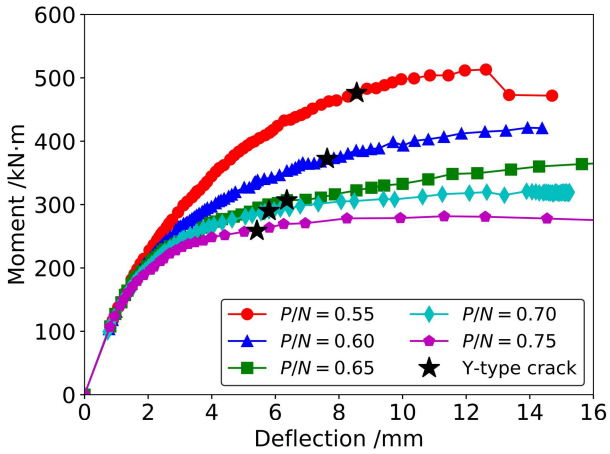

611

612 Fig. 16. Curves of bending moment versus deflection under different loading paths.

613

614

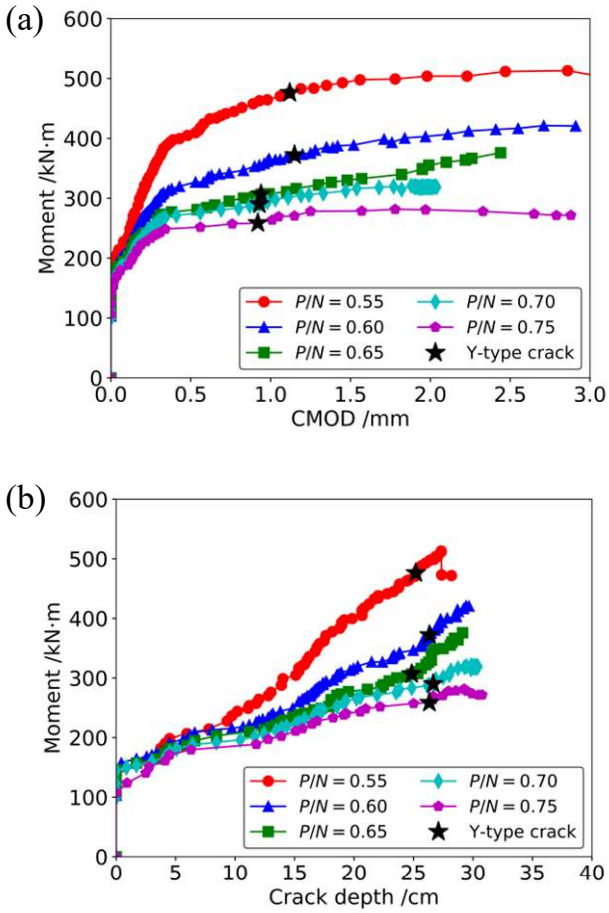

615

616

617 Fig. 17. Relationship between crack evolution and bending moment. (a) CMOD; (b) Crack depth.

618

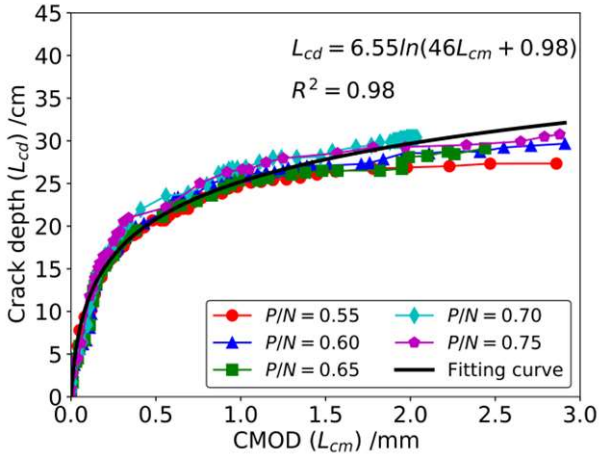

Fig. 18. Relationship between crack depth and CMOD.